RSC Advances

PAPER

View Article Online
View Journal | View Issue

Cite this: *RSC Adv.*, 2017, **7**, 45595

Tailoring the performance of magnetic elastomers containing Fe_2O_3 decorated carbon nanofiber†

Dongju Lee,‡[a] O.-Seok Kwon‡[b] and Sung Ho Song *[c]

One important strategy for developing high performance smart materials is to utilize the magnetic properties of elastomers. Here we prepared magnetic elastomer nanocomposites using the latex compounding method followed by *in situ* methods. Our strategy exploited the synergetic effect of carbon nanofibers (CNFs) and ferric oxide (Fe_2O_3), which, when combined, can improve the dispersion within the elastomer matrix by introducing hybrid nanomaterial networks. When Fe_2O_3 decorated CNFs (CNF–Fe_2O_3) were embedded in an SBR matrix, they produced a remarkable improvement in the composite material's mechanical and thermal properties. This was attributed to the efficient dispersion of the CNF–Fe_2O_3, and the enhanced interfacial interaction between the filler particles and the elastomer matrix. Furthermore, the magnetic properties of the elastomer nanocomposites were modulated by the addition of the prepared CNF–Fe_2O_3 hybrids. The synergistic reinforcement of SBR achieved by the incorporation of CNF–Fe_2O_3 hybrids can support the development of high performance magnetic elastomers for applications in electronic appliances, magnetoresistive sensors, actuators, and automotive parts.

Received 10th August 2017
Accepted 19th September 2017

DOI: 10.1039/c7ra08861b

rsc.li/rsc-advances

1. Introduction

In the past decade there has been intense research interest in smart materials, which are characterized by the ability to be significantly changed in a controlled fashion by external stimuli.[1,2] Among the various types, magnetic elastomers (MREs), are smart materials whose mechanical properties can be changed in a controlled manner by an applied magnetic field.[3] MREs currently play crucial roles in various applications including automobiles, architecture and as vibration absorbers.[4] However, because magnetic nanoparticles experience some problems, such as particle sedimentation, there has been increasing interest in the development of MREs, which can be formed by dispersing magnetic particles in a solid medium, such as gels and elastomers, including silicon rubber, natural rubber, polyurethane sealant, acrylonitrile and polybutadiene.[5,6] Since the performance of the MREs strongly depends on the magnetic and mechanical properties of the MRE materials, it is essential to understand the relative effects of the magnetic particles and the matrix on these properties.

Previous studies have noted that the magnetic properties of MREs increase with increasing magnetic particle content, but this also degrades their mechanical properties. The decline in mechanical properties has been attributed to weak adhesion between the magnetic fillers and the elastomer matrix.[7–9] To improve the interfacial interaction between the magnetic filler and the polymer matrix, the surface energy of the fillers must be greater than or equal to the surface energy of the polymer. Large sized magnetic particles exhibit a small intrinsic surface energy, and are apparently unable to form strong bonds with the elastomers.[6] For this reason, to improve the interfacial bonding, surface modification methods and nano-sized particles have been employed to effectively increase the surface energetics of the magnetic particles.

In recent years, a number of studies have demonstrated that when two geometrically dissimilar nanomaterials are incorporated in an elastomer matrix, significant synergistic effects can occur which can improve the properties of the composites. In particular, hybrid fillers consisting of two different types of nanomaterials have exhibited remarkable synergetic benefits, and have been used to enhance the properties of nanocomposites. Such hybrid nanomaterial networks have also been found to prevent the formation of undesirable self-aggregation, which is detrimental to the properties of the composites.[10]

In this study, we successfully manufactured CNF–Fe_2O_3 based multifunctional styrene butadiene rubber (SBR) nanocomposites. Among various types of rubber, SBR has

[a]*Department of Advanced Materials Engineering, Chungbuk National University, Chungdae-ro 1, Seowon-Gu, Cheongju, Chungbuk 34057, Republic of Korea*

[b]*NEXEN Tire Corporation R&D Center, 30, Yusan-Dong, Yangsan-Si, Kyungnam, Korea 626-230*

[c]*Division of Advanced Materials Engineering, Kongju National University, Chungnam 330-717, Republic of Korea. E-mail: shsong805@gmail.com*

† Electronic supplementary information (ESI) available: SEM images of CNF–Fe_2O_3 and composites, XPS spectra of CNFs, formation of elastomer composites. See DOI: 10.1039/c7ra08861b

‡ These authors contributed equally.

mechanical characteristics more suitable for an MR elastomer matrix material than others. Also, Fe_2O_3 nanoparticles are one of the most commonly used magnetic nanoparticles. Carbon nanofibers (CNF), which have low manufacturing cost and outstanding mechanical, electrical, and thermal properties, are also promising candidates for developing novel structural materials. A master batch of CNF–Fe_2O_3/SBR was prepared to improve the dispersion of the nanoparticles in the elastomer latex matrix, and the as-prepared hybrid nanomaterials were incorporated into the SBR through latex co-coagulation. The elastomer nanocomposites with CNF–Fe_2O_3 exhibited excellent mechanical, fatigue, thermal, electrical and magnetic properties. These multifunctional elastomer nanocomposites have potential applications in electronic appliances, magneto-resistive sensors, actuators, and automotive parts.

2. Experimental section

2.1 Materials

The matrix material was selected styrene butadiene rubber (SBR 1500, Kumho Petrochem Co. Ltd., Korea) consisting of styrene of 23% and butadiene of 77%. The carbon black (N-330, OCI Co. Ltd., Korea), *N-tert*-butyl-benzothiazole sulfonamide (TBBS, ShangdongShanxian Co. Ltd., China) were used and zinc oxide (ZnO), stearic acid (S/A), sulfur, and oleic acid were purchased from Sigma-Aldrich. Carbon nanofibers (CNF), which have 95% purity, outside diameter of 200–500 nm and length ranging from 10 to 40 μm, used in this study were purchased from Nanostructured and Amorphous Materials, Inc. USA. The ferric nitrate $Fe(NO_3)_3 \cdot 9H_2O$ ethanol (98% purity) were also purchased from Sigma-Aldrich.

2.2 Preparation of hybrid nanomaterials

For the introduction of functional groups, the commercial carbon nanofiber was pretreated in concentrated HNO_3–H_2SO_4 (4 : 1, v/v) solution at 85 °C for 5 h, intensively washed with deionized water and dried in vacuum. Ferric oxide (Fe_2O_3) from $Fe(NO_3)_3 \cdot 9H_2O$ was impregnated onto 5 g of the CNFs in ethanol, followed by sonication (110 V at 40% amplitude) and calcination at 350 °C for 3 h. For 10% iron oxide 1.443 g of $Fe(NO_3)_3 \cdot 9H_2O$ was dissolved in 300 ml ethanol. An amount of 1.8 g of CNF was also dissolved in 400 ml of absolute ethanol. Both solutions were sonicated for 45 min separately and then mixed together. The resultant mixture was again sonicated for 1 h at room temperature. The mixture was then kept in an oven to evaporate the ethanol. The aim of ultrasonication is to have a complete and homogeneous wetting of the particles during impregnation and hence decreasing the possibility of agglomeration due to the formation of clumps of liquid. The residue was then calcined for 3.5 h at 350 °C in furnace to get CNF impregnated with Fe_2O_3.

2.3 Preparation of elastomer nanocomposites

The CNF–Fe_2O_3 hybrids/SBR nanocomposites were prepared by following standard procedures in Table S1.† First, the SBR latex (20 phr) with 5 phr (parts per hundred rubber by weight) carbon black, Fe_2O_3, CNF, and hybrid nanomaterials CNF–Fe_2O_3 were mixed by vigorous stirring for 24 h, respectively. During coagulation, butadiene–styrene–vinyl-pyridine rubber (VPR) was added to a small loading, and VPR not only plays a key role in the prevention of aggregation of CNF–Fe_2O_3 but also acts as an interface-bridge between CNF–Fe_2O_3 and SBR. The nanomaterials/SBR emulsion was then coagulated by a 1.0 phr sulfuric acid solution. The coagulated composites were washed with water until the pH of the filtered water reached 6–7 and then dried in an oven at 50 °C for 24 h. And then, the SBR 80 phr and carbon materials (5 phr)/SBR emulsion (20 phr) were mixed in Banbury mixer at a rotor speed of 60 rpm for mater batches. The additives and vulcanization agents were added at the end so that curing process of the mixture could be started. The compounds were placed in the aluminum mold and cured at 160 °C for T90 by rheometer under pressure. The formulations of the diver nanomaterials/SBR composites are summarized in Table S1.†

2.4 Characterization

The crystallographic structures of the samples were analyzed by X-ray diffraction (D/MAX-2500 (18 kW)) with Cu Kα radiation (λ = 1.518 Å). A thermogravimetric analysis (TGA) was performed using a G209F3 at a heating rate of 10 °C min^{-1} under a N_2 atmosphere. Scanning electron microscopy (SEM, JEOL JSM-6490LV) was used to observe the morphology of the fractured surface of elastomer nanocomposites and nanomaterials. The specimens were fractured in liquid nitrogen and the cross surface of samples were coated by gold using a sputtering process. Tensile tests were carried out in an Instron tensile machine (Instron Co., UK) at crosshead speed of 300 mm min^{-1}. The dumbbell shape samples were 100 mm in thickness and 5 mm in width. At least four tests were carried out for each case. Raman spectra were obtained from 1200 to 3000 cm^{-1} using a Raman spectrometer (LabRAM HR UV/Vis/NIR, excitation at 514 nm). The magnetic properties of elastomer nanocomposites were investigated at room temperature using a physical property measurement system (PPMS-9, Quantum Design) equipped with a 4 T vibrating sample magnetometer (VSM).

3. Results and discussion

Fig. 1a illustrates the synthetic routes for synthesizing Fe_2O_3 decorated CNF (CNF–Fe_2O_3). The main concept for preparing a CNF–Fe_2O_3/SBR based magnetic elastomer with good mechanical properties is to increase the dispersion of the fillers by promoting interfacial interactions between the Fe_2O_3 and CNFs. To prepare CNF–Fe_2O_3 hybrids, the CNFs were covalently functionalized by treatment in an acidic environment, followed by the *in situ* growth of Fe_2O_3 on the CNF surfaces. In the CNF–Fe_2O_3 hybrid, the Fe_2O_3 nanoparticles are linked to the CNF surface by covalent bonding. The morphologies of the prepared CNFs and CNF–Fe_2O_3 hybrids were investigated by scanning electron microscopy (SEM), and their SEM images are shown in Fig. 1b and c, respectively. The SEM images of the CNFs show them to be randomly oriented with a smooth and uniform

surface (Fig. 1b). The diameters of the pure CNFs ranged from 150 nm to 300 nm. Fig. 1c and S1† show the SEM image of the synthesized CNF–Fe_2O_3 hybrids. Although a minor degree of aggregation occurred, most of the Fe_2O_3 nanoparticles are bound to the surface of the CNFs. The extensive coverage by the Fe_2O_3 nanoparticles is attributed to oxygenated functional groups or surface defects produced by acid treatment on the surface of the CNFs. Such defects are thermodynamically favorable nucleation sites, which tend to facilitate the nucleation and growth of the nanoparticles.[11,12]

The morphology and structure of the CNF–Fe_2O_3 hybrids were also investigated in detail by transmission electron microscopy (TEM). Fig. 2a shows a typical TEM image of the CNF–Fe_2O_3 and Fig. 2b and c present higher magnification TEM images. In the low-magnification TEM image (Fig. 2a), all of the Fe_2O_3 nanoparticles are supported on the CNFs, and appear as small dark dots. There are no free nanoparticles around the CNFs. Typical TEM images (Fig. 2b and c) show clearly that the CNF is decorated by Fe_2O_3 nanoparticles, whose diameters range from 5–10 nm. The distribution of Fe_2O_3 nanoparticles on the surface of the CNF is uniform, and no aggregated or free particles are detected, suggesting a strong interaction between the Fe_2O_3 nanoparticles and CNFs. The HRTEM image (Fig. 2d) indicates the high crystallinity of the nanoparticles. The lattice spacing between two adjacent crystal planes of the particles was determined to be 0.25 nm, corresponding to the (110) lattice plane of α-Fe_2O_3.

The prepared hybrids were then further analyzed using XPS to verify the interaction between the nanoparticles and the CNF supports. Fig. 3 and S2† show the XPS spectra of the CNF–Fe_2O_3 hybrids and acid-treated CNFs. As seen in Fig. 3a and S2a,† the survey scan spectra of the hybrids exhibit peaks at binding energies of 285, 530 and 711 eV, which are attributed to C1s, O1s and Fe2p, respectively. In contrast, only C1s and O1s peaks can be observed from the acid-treated CNFs in Fig. S2.† An obvious Fe2p (711 eV) peak can be found in the hybrids, which

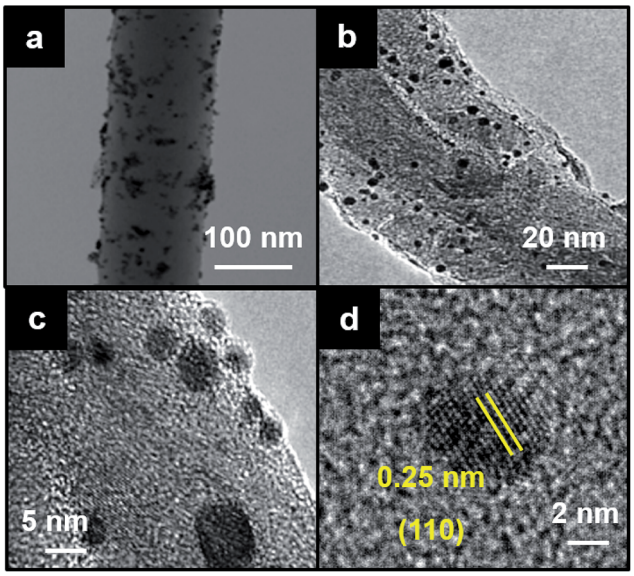

Fig. 2 (a) Low-magnification TEM image of CNF–Fe_2O_3 hybrids. (b and c) Higher magnification of TEM images of CNF–Fe_2O_3 hybrids. (d) HRTEM image of Fe_2O_3 nanoparticle onto CNF surface.

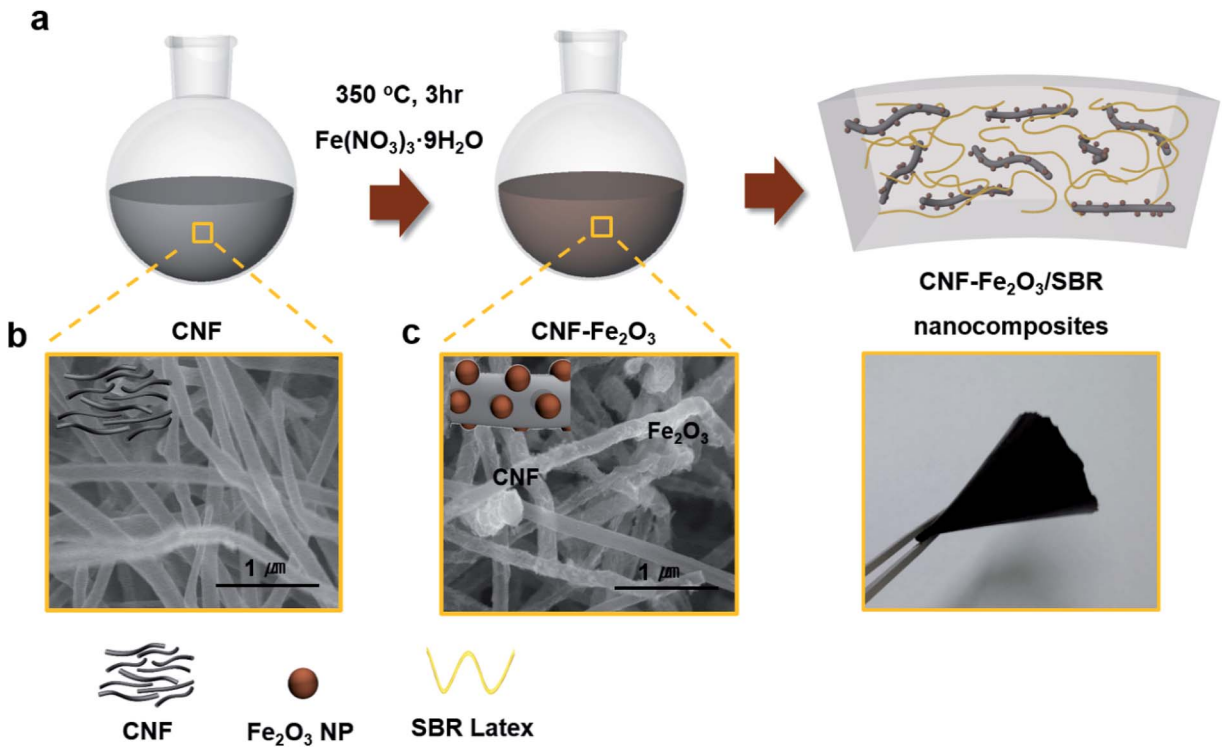

Fig. 1 (a) Schematic illustration of *in situ* synthesizing CNF–Fe_2O_3 hybrids and CNF–Fe_2O_3 hybrids incorporated nanocomposites. SEM image of (b) CNF and (c) the CNF–Fe_2O_3 hybrids.

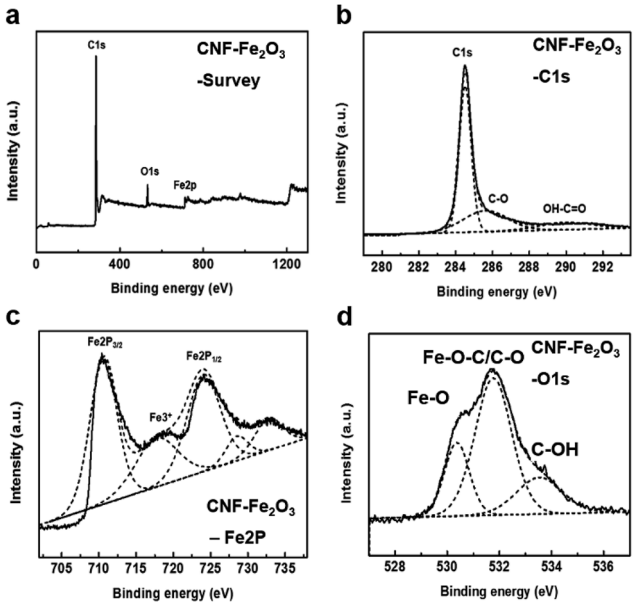

Fig. 3 High resolution XPS spectra of the CNF–Fe_2O_3 hybrids on silicon oxide substrates. (a) Survey scan, (b) C1s scan, (c) O1s scan, and (d) Fe2p scan.

provides evidence of the successful deposition of the Fe_2O_3 nanoparticles onto the CNFs. From the C1s narrow scan (Fig. 3b), the C1s spectra of the hybrids can be fitted to the mainly C–C bonds in aromatic rings (284.6 eV), C–O (286.1 eV) and C=O–OH (289.0 eV).[13,14] From the Fe2p narrow scan (Fig. 3c), the peaks of $Fe2p_{3/2}$ and $Fe2p_{1/2}$ (711.2 and 724.5 eV) observed in the hybrids are the characteristic positions of Fe_2O_3. The formation of Fe–C bond can be excluded from the C1s and Fe2p spectra of the hybrids, since Fe–C bonds would be present at 283.3 eV and 717.5 eV, respectively.[15,16]

In Fig. S2b,† the C1s signal of the acid treated CNFs consists of four different peaks: the C–C bond (284.5 eV) of sp^2 carbon, a C–O bond (286.6 eV), C=O groups (288.2 eV), and the OH–C=O bond (290.1 eV). Also, the O1s spectrum of the acid-treated CNF can be deconvoluted into three peaks, O–O at 530.5 eV, C=O at 532.5 eV, and O=C–OH at 533.5 eV in Fig. S2c.†[17] The deconvolution of the O1s spectrum of the hybrids consists of three peaks, at 530.9, 531.5, and 533.9 eV (Fig. 3d). The peaks at 530.9 eV correspond to the Fe–O bond coming from Fe_2O_3, and the component at 533.9 eV was assigned to the oxygen group in the CNFs. The peak at 531.5 eV in the hybrids spectra could be caused by the bond of Fe–O–C, formed between the CNF and Fe_2O_3 and/or the C–O group from the CNF, because the binding energy of C–O is very close to this peak. This result was also confirmed in the results in previous reports, which found that the binding energy of O1s in the Fe–O–C bond can be present in the range of 531–533 eV.[11,15,18] Accordingly, that peak should be attributed mainly to the Fe–O–C bond formed between the CNF and Fe_2O_3.

Fig. 4a indicates the X-ray diffraction (XRD) patterns of the CNFs, and CNF–Fe_2O_3 hybrids. The pattern shows an intense peak at $2\theta = 26.5^\circ$ corresponding to the (002) reflection. The XRD pattern of the hybrids also indicates that all of the diffraction peaks are very sharp and are indexed well with pure α-Fe_2O_3, indicating the highly crystalline structure and the high phase purity of the Fe_2O_3. The strong diffraction peaks at about 21°, 34°, 36°, 42°, 54°, 63°, 65° and 72° correspond to the (012), (104), (110), (113), (116), (122), (213) and (300) crystal planes of Fe_2O_3, respectively. The thermogravimetric analysis (TGA) results shown in Fig. 4b, for CNF indicate there is a dramatic mass loss at 650 °C, which can be attributed to the oxidation of CNF and the emission of CO_2/CO gas. However, for the hybrids, the oxidation temperature was dramatically reduced to only 220 °C. This is because the Fe_2O_3 nanoparticles in the hybrids can accelerate the oxidation of CNFs. When Fe_2O_3 is in tight contact it can effectively promote the oxidation of carbon, even though when it is in loose contact it results in hardly any activity.[19,20] It is well known that the type of contact (loose or tight contact) between metal/metal oxide catalysts and carbons are the key factors affecting the oxidation reactivity of carbon over catalysts.[15] Therefore, this result indicates that there is close interfacial interaction between the Fe_2O_3 and CNF. Measurements further revealed that the zeta potential magnitude of the hybrids significantly decreased from −79 mV to −50 mV after synthesis with the nanoparticles (Fig. 4c). This decrease is closely related to the removal of oxygen functional groups by the nucleation and growth of nanoparticles at the sites of the oxygen functional groups, to form Fe–O–C.

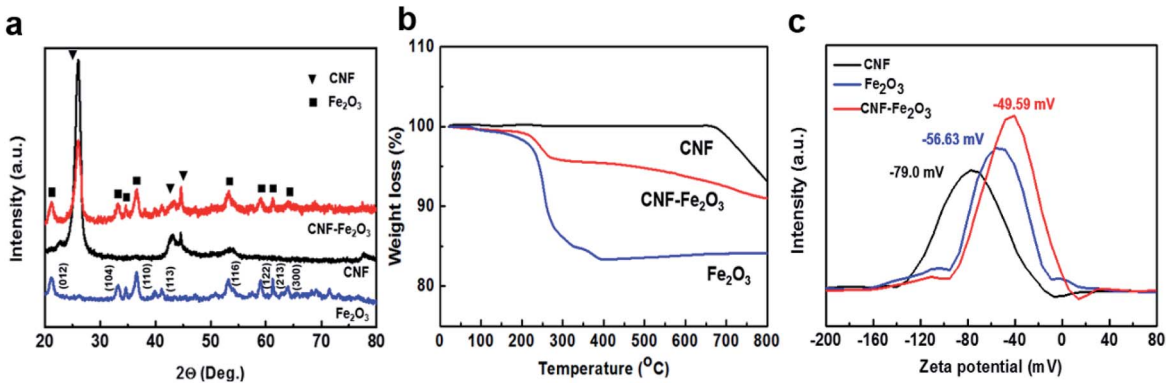

Fig. 4 Characterization of the CNF–Fe_2O_3 hybrids. (a) XRD, (b) TGA, and (c) zeta potential results.

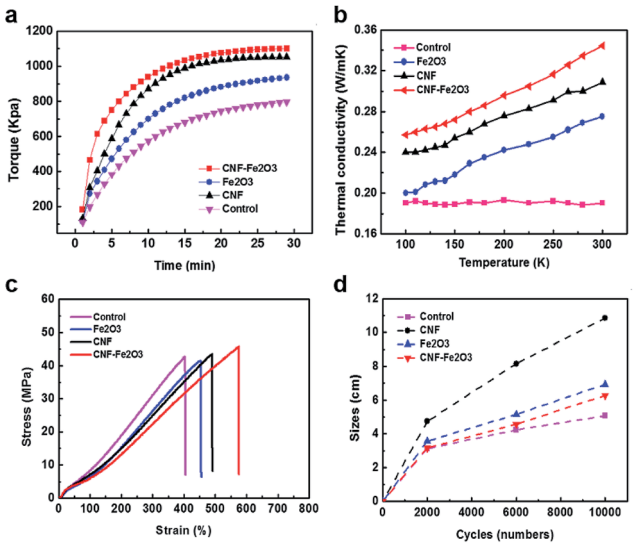

Fig. 5 (a) Curing properties, (b) thermal conductivities, (c) mechanical properties and (d) crack length *versus* fatigue cycles and its fatigue lifetimes of the SBR composites.

The SBR nanocomposites with different embedded fillers were prepared as an optimization condition in Fig. S3.† The curing curves of the CNF–Fe_2O_3 hybrids and other material embedded rubber composites are shown in Fig. 5a. All of the rubber composites show two different regions: (i) the vulcanizing region when the curing reaction occurs, leading to a sharp increase in torque with the formation of a network structure; and (ii) a plateau in the curing curve when the network is stabilized as it reaches equilibrium.[21] The significant increase in torque reveals the excellent reinforcing effect of the CNF–Fe_2O_3 on the SBR composites. Additionally, the enhanced vulcanization rate reduced the curing time, which helps to minimize potential losses in the magnetic properties of the Fe_2O_3.[22] The thermal conductivity of the composites was investigated at temperatures (T) ranging from 100 to 300 K, and the results are shown in Fig. 5b. The thermal conductivity of the CNF–Fe_2O_3/SBR nanocomposites decreases nearly linearly as T decreases from 300 to 100 K, and other rubber composites also exhibit similar trends. This linear temperature dependent behavior is consistent with Umklapp phonon scattering, which is characteristic of crystalline materials.[23,24] Pure SBR samples did not exhibit any apparent temperature dependence over the same temperature range. Fig. 5c presents the typical stress–strain curves of the SBR composites with different embedded fillers. As shown in Fig. 5c, the elongation at break of the CNF–Fe_2O_3/SBR nanocomposites is remarkably increased, possibly arising from the slipping of the rubber chains along the CNFs during tensile stretching. Compared to the neat SBR, the CNF–Fe_2O_3/SBR nanocomposites showed an increase in elongation of 42%. The CNF–Fe_2O_3 hybrids provided a significant enhancement in the area under the curves, indicating enhanced ductility. This performance enhancement was due to the SBR, which has a flexible cross-linking network, and the improved dispersion of the hybrids within the elastomer matrix. SEM images of the fracture surfaces of the elastomer nanocomposites after the tensile tests are shown in Fig. S3.† The CNF–Fe_2O_3/SBR nanocomposites exhibit roughened fractured surfaces, indicating stronger interfacial adhesion between the CNF–Fe_2O_3 and SBR matrix. The ultimate tensile strength of the nanocomposites with CNF–Fe_2O_3 hybrids was increased by as much as 10% and 12% relative to that of CNF and Fe_2O_3 nanocomposites, respectively. The fatigue properties of the nanomaterials/SBR composites are presented in Fig. 5d. It is noted that the CNF–Fe_2O_3/SBR nanocomposites exhibited a remarkable reduction in crack length, even after 10 000 cycles, and the fatigue crack growth ($dc/dn = AG^{\alpha}$; c is the crack length, n is the cycles, and G is the tear energy) of the CNF–Fe_2O_3/SBR nanocomposites (2.07) decreased by over 81%, compared to those of the CNF/SBR (3.76) and Fe_2O_3/SBR (2.29). This is because the hybrid nanomaterial networks prevented the formation of undesirable self-aggregation, which is detrimental to the properties of the composites. The presence of filler clusters can induce stress concentration, which can easily produce crack initiation and propagation, and reduce the efficiency of stress transfer between the matrix and the filler, thus lowering the reinforcing effect.[25]

Fig. 6a displays the magnetization curves of the CNF, Fe_2O_3, and CNF–Fe_2O_3 hybrids at room temperature. The paramagnetic response of the Fe_2O_3 sample is apparent. The near-zero coercivity and remanence of the magnetization curves indicate that the CNF and CNF–Fe_2O_3 hybrids are superparamagnetic in nature. The saturation magnetization values

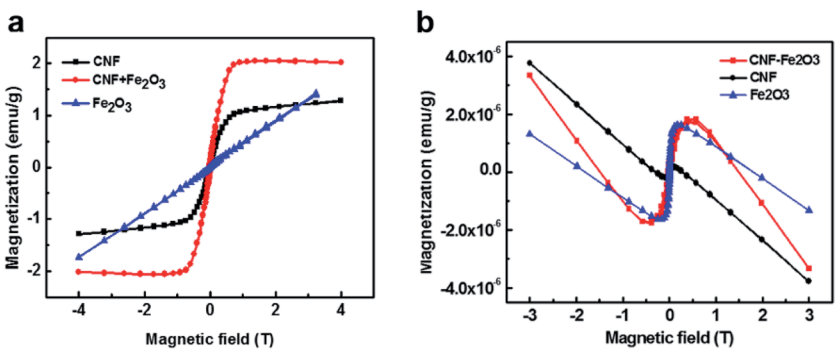

Fig. 6 Magnetization of (a) CNF, Fe_2O_3, and CNF–Fe_2O_3 hybrids and (b) SBR composites with diverse fillers.

(M_s) for the CNFs and the CNF–Fe_2O_3 composite were found to be 1.11 and 2.08 emu g^{-1}, respectively. The magnetization curve of the SBR rubber exhibits diamagnetic behavior as shown in Fig. 6b. However, following the addition of the filler, there is a paramagnetic contribution, with different specific saturation induction properties, that can be clearly observed after subtracting the diamagnetic background.[26] It can be concluded that the magnetic properties of the elastomer nanocomposites can be finely tuned by decorating the surface of CNFs with Fe_2O_3 nanoparticles.

4. Conclusion

In summary, we have demonstrated that CNFs decorated with *in situ* synthesized Fe_2O_3 nanoparticles can be integrated into an elastomer matrix using the latex compounding method. In this study Fe_2O_3 nanoparticles were contacted with CNFs *via* Fe–O–C bonds, and the *in situ* method reduced Fe_2O_3 agglomeration and produced a uniform dispersion of Fe_2O_3 nanoparticles in the SBR matrix. The CNF–Fe_2O_3 embedded elastomer composites showed improved mechanical and thermal properties, which resulted from the interfacial adhesion between the CNF–Fe_2O_3 and SBR matrix and their improved dispersion within the elastomer matrix by hybrid nanomaterials networks. Moreover, the magnetic properties of the elastomer were modulated by the addition of the CNF–Fe_2O_3 hybrids. These results strongly indicate that the mechanical and magnetic properties of the rubber can be simultaneously improved by decorating CNF fillers with Fe_2O_3 nanoparticles. The results of this research suggest that the proposed technique can be useful in the development of high performance magnetic rubber composites for potential electronic appliances, automotive parts, and magnetostrictive actuators.

Conflicts of interest

There are no conflicts to declare.

References

1 E. Y. Kramarenko, A. V. Chertovich, G. V. Stepanov, A. S. Semisalova, L. A. Makarova, N. S. Perov and A. R. Khokhlov, *Smart Mater. Struct.*, 2015, **24**, 035002.
2 A. Sahbi and K. Manfred, *Smart Mater. Struct.*, 2015, **24**, 025016.
3 H. S. Jung, S. H. Kwon, H. J. Choi, J. H. Jung and Y. G. Kim, *Compos. Struct.*, 2016, **136**, 106–112.
4 S. Kruti, P. Do Xuan, S. Min-Sang, R. V. Upadhyay and C. Seung-Bok, *Smart Mater. Struct.*, 2014, **23**, 027001.
5 L. Chen, X.-L. Gong, W.-Q. Jiang, J.-J. Yao, H.-X. Deng and W.-H. Li, *J. Mater. Sci.*, 2007, **42**, 5483–5489.
6 Y. Sun, X. Zhou, Y. Liu, G. Zhao and Y. Jiang, *Mater. Res. Bull.*, 2010, **45**, 878–881.
7 M. Brzozowska and P. Krysinski, *Electrochim. Acta*, 2009, **54**, 5065–5070.
8 A. Poddar, R. N. Bhowmik, A. De and P. Sen, *J. Magn. Magn. Mater.*, 2009, **321**, 2015–2020.
9 T. Iwamoto, Y. Kitamoto and N. Toshima, *Phys. B*, 2009, **404**, 2080–2085.
10 P.-C. Ma, M.-Y. Liu, H. Zhang, S.-Q. Wang, R. Wang, K. Wang, Y.-K. Wong, B.-Z. Tang, S.-H. Hong, K.-W. Paik and J.-K. Kim, *ACS Appl. Mater. Interfaces*, 2009, **1**, 1090–1096.
11 N. A. Zubir, C. Yacou, J. Motuzas, X. Zhang and J. C. Diniz da Costa, *Sci. Rep.*, 2014, **4**, 4594.
12 Z. Geng, Y. Lin, X. Yu, Q. Shen, L. Ma, Z. Li, N. Pan and X. Wang, *J. Mater. Chem.*, 2012, **22**, 3527–3535.
13 S. Byun, J. H. Kim, S. H. Song, M. Lee, J.-J. Park, G. Lee, S. H. Hong and D. Lee, *Chem. Mater.*, 2016, **28**, 7750–7756.
14 J. Kim, S. H. Song, H.-G. Im, G. Yoon, D. Lee, C. Choi, J. Kim, B.-S. Bae, K. Kang and S. Jeon, *Small*, 2015, **11**, 3124–3129.
15 J. Zhou, H. Song, L. Ma and X. Chen, *RSC Adv.*, 2011, **1**, 782–791.
16 A. Adenier, M.-C. Bernard, M. M. Chehimi, E. Cabet-Deliry, B. Desbat, O. Fagebaume, J. Pinson and F. Podvorica, *J. Am. Chem. Soc.*, 2001, **123**, 4541–4549.
17 A. J. Plomp, D. S. Su, K. P. D. Jong and J. H. Bitter, *J. Phys. Chem. C*, 2009, **113**, 9865–9869.
18 X. Xu, H. Li, Q. Zhang, H. Hu, Z. Zhao, J. Li, J. Li, Y. Qiao and Y. Gogotsi, *ACS Nano*, 2015, **9**, 3969–3977.
19 J. P. A. Neeft, M. Makkee and J. A. Moulijn, *Chem. Eng. J. Biochem. Eng. J.*, 1996, **64**, 295–302.
20 J. P. A. Neeft, M. Makkee and J. A. Moulijn, *Appl. Catal., B*, 1996, **8**, 57–78.
21 S. H. Song, J. M. Kim, K. H. Park, D. J. Lee, O. S. Kwon, J. Kim, H. Yoon and X. Chen, *RSC Adv.*, 2015, **5**, 81707–81712.
22 Y. Chen, X. Huang, Z. Gong, C. Xu and W. Mou, *Ind. Eng. Chem. Res.*, 2017, **56**, 183–190.
23 O. S. Kwon, D. Lee, S. P. Lee, Y. G. Kang, N. C. Kim and S. H. Song, *RSC Adv.*, 2016, **6**, 59970–59975.
24 S. H. Song, K. H. Park, B. H. Kim, Y. W. Choi, G. H. Jun, D. J. Lee, B. S. Kong, K. W. Paik and S. Jeon, *Adv. Mater.*, 2013, **25**, 732–737.
25 N.-J. Huang, J. Zang, G.-D. Zhang, L.-Z. Guan, S.-N. Li, L. Zhao and L.-C. Tang, *RSC Adv.*, 2017, **7**, 22045–22053.
26 S. K. Srivastava, *Natural Rubber Materials: Volume 2: Composites and Nanocomposites*, The Royal Society of Chemistry, 2014.

